NANO: Brief Reports and Reviews
Vol. 2, No. 5 (2007) 285–294

World Scientific
www.worldscientific.com

CHARGE TRANSPORT THROUGH CARBON NANOTUBE OR FULLERENE–MOLECULE–SILICON JUNCTIONS

FU-REN F. FAN*, BO CHEN†, AUSTEN K. FLATT†, JAMES M. TOUR†,‡ and ALLEN J. BARD*,§
*Center for Electrochemistry
Department of Chemistry and Biochemistry and
Center for Nano- and Molecular Science
The University of Texas at Austin, Austin
Texas 78712, USA

†Department of Chemistry and
Center for Nanoscale Science and Technology
Rice University, Houston, Texas 77005, USA
‡tour@rice.edu
§ajbard@mail.utexas.edu

Received 29 August 2007
Revised 21 September 2007

We report here the current–voltage (i–V) characteristics of several (n^{++}-Si/MNOPE/C_{60}/Pt-tip) or (n^{++}-Si/MNOPE/SWCNT/Pt-tip) junctions, where MNOPE = 2'-mononitro-4, 4'-bis(phenylethynyl)-1-phenylenediazonium and SWCNT = single wall carbon nanotube. A layer of C_{60} or SWCNT-derivatized MNOPE has strong effect on the i–V behavior of the junctions, including rectification, negative differential resistance (NDR) and switching behaviors. The i–V curve of a grafted molecular monolayer (GMM) of MNOPE atop n^{++}-Si shows NDR behavior, whereas those of C_{60}- and SWCNT-derivatized GMMs of MNOPE on n^{++}-Si show strong rectifying behavior with opposite rectification polarities. With C_{60}, larger currents were found with negative tip bias, while with SWCNT, the forward top bias was positive. Because C_{60} tends to be a good electron acceptor and SWCNTs tend to be good electron donors, they show different i–V behavior, as observed. Some of the (n^{++}-Si/MNOPE/SWCNT/Pt-tip) junctions also show reversible bistable switching behavior.

Keywords: Molecular electronics; grafted molecular layer; rectification; bistable switching; fullerene; single wall carbon nanotube.

1. Introduction

Traditionally, molecular electronic efforts have been driven by thiol-gold chemistry to molecules bonded to gold substrates.[1] Significant advances are being made in developing an improved understanding of the mechanisms that determine the electrical transport properties in molecular junctions with metal. Although the choice of molecule plays a critical role in the operation of metal–molecule–metal junctions, the interface between the molecule and the electrodes has come under increasing scrutiny due to limited agreement between experimental

and theoretical analyses.[2] The apparent importance of the contacts in molecular electronic devices suggests that alternative electrode materials and multi-layer structure of different compounds may lead to unique charge transport phenomena. For example, several recent experiments have demonstrated the feasibility of attaching various molecules on silicon surfaces and showed different electrical transport properties, e.g., NDR, rectification and switching.[3] Recent advances in "wet" surface chemistry offer an increasingly sophisticated range of techniques for self-orienting molecular chemisorption on a wide variety of materials. Most recently, Tour and coworkers have demonstrated covalent attachment of arenes via aryldiazonium salts to hydride-passivated Si surface[4] and fabricated single wall carbon nanotube (SWCNT) or fullerene C_{60}/molecule/silicon junctions.[5] Furthermore, these junctions proved to provide stable contacts for new molecular electronic memory devices. Therefore, the interface of molecules to silicon may provide a transition step for the introduction of molecules into more traditional device platforms for molecular electronics research. In this report, we compare the charge transport properties of three different (SWCNT or C_{60}/MNOPE/n^{++}-Si) junctions, which reflect the importance of the interfacial energetics for electron transfer to the performance of molecular electronics.

2. Experimental Section

The experiments were performed on Si(111) substrates, which were degenerately n-type doped with arsenic with a resistivity of $< 0.005\,\Omega$-cm. The silicon wafer was first cleaned for 30 min in 2:1 H_2SO_4/H_2O_2 (piranha solution) followed by rinsing copiously with water and drying in a stream of N_2. The wafer was then hydride-terminated by immersion in Ar-sparged concentrated (40%) NH_4F for 15 min, rinsed with water, and dried in a stream of N_2. In a typical experiment for molecular attachment, the target molecule (containing a diazonium salt on one end and an aniline moiety on the other end) in anhydrous CH_3CN (0.5 mM) was exposed to a hydride-passivated Si(111) surface according to the procedures reported previously[4,5] in a nitrogen-filled glovebox for the desired reaction time. Following monolayer assembly, the substrate was removed from the glovebox and placed in a 0.3 M solution of isoamylnitrite in CH_3CN for 5 min to diazotize the terminal aniline. The substrate was then removed and immediately immersed in an aqueous SWCNT/sodium dodecyl sulfate (SDS) suspension (0.7 μM) at pH 10 for 24 h, or fullerene in chlorobenzene solution for 14 h. Following fullerene or SWCNT (the diameter of SWCNT ranges from 0.95 to 3.1 nm) attachment, the substrate with GMMs was removed, rinsed with water and CH_3CN for SWCNT attachment and with chlorobenzene for fullerene attachment, and dried with a stream of nitrogen. The prepared sample was then characterized by ellipsometry, XPS and atomic force microscopy (AFM) prior to electrical measurement. The C_{60} coverage was monolayer with the thickness increase of about 7 Å, and XPS analysis showed great increase of atomic concentration of C1s signal. The AFM image showed a high coverage of SWCNTs (~ 5 tubes/μm^2) connected to the silicon substrate via the MNOPE molecules.[5]

The i–V curves were measured with a custom-built tuning fork-based scanning probe microscope (SPM)[6] and the systematic representation of an (n^{++}-Si/MNOPE/SWCNT/Pt-tip) junction is shown in Scheme I. The gain of the current preamplifier was set at a value of 10^{10}, which limits the magnitude of the measured current range to 1 nA. Current values exceeding this threshold result in saturation of the detector, as observed in some of the i–V measurements near the upper and lower bounds of the sweep voltage.

A constant current suppression of a few tenth of pA was sometimes used to correct for the offset of the current amplifier. An electrochemically etched Pt or Ir-Pt (20–80%) wire serving as the tip is glued along the side of one of the prongs of a quartz crystal tuning fork. Although very sharp tips were usually used for electrical measurements, relatively

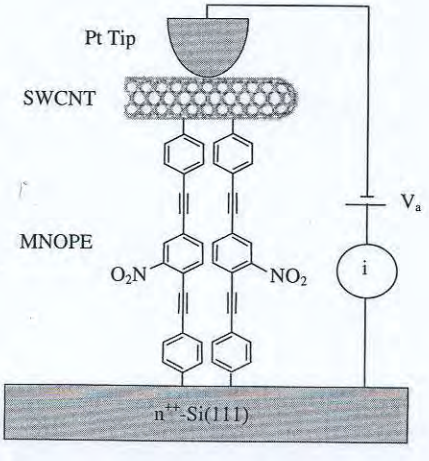

Scheme I

blunt tips (radius of curvature $\geq 2\,\mu$m) were used for C_{60} or SWCNT-derivatized GMMs to increase the probability that the tip would be on the top of at least one C_{60} or SWCNT during measurement. As the tip approaches the surface of a substrate, the amplitude and frequency of the oscillation of the tuning fork decrease as soon as the tip just contacts the GMM surface and this can be used to sense the presence of the surface. Thus, the tip can be moved to the substrate and positioned fairly rapidly. The tip is then retracted slightly ($\sim$10–20 nm) and moved to a different location of the GMM. The SPM is then operated in the current-measurement mode as a function of voltage or distance with the feedback loop turned off. The i–V curves were obtained by sweeping the potential of the tip with respect to the Si substrate at a scan rate of 6 V/s over the desired potential range and recording the current, as the tip again approached toward the GMM, this time in small steps (1.0–3.5 Å each step). We measured the current that flowed across the GMM in response to changes in bias voltage while the tip approached stepwise towards the surface of a GMM on Si. Before the tip contacts the GMM surface, no current in excess of the noise level ($\sim$0.2 pA) flowed. The constant background current observed during voltage scan is mainly associated with the capacitive charging of the system. When a current greater than a few times the noise level flowed across the GMM, the first and several subsequent i–V curves were recorded. All measurements were carried out at room temperature (25.0 $\pm$ 0.5°C) under dried argon in the dark.

3. Results and Discussion

Figure 1 shows a series of i–V curves taken at three different distances as the tip approaches a hydrogen-terminated bare n^{++}-Si(111) surface. Those curves are relatively featureless and nearly symmetric, as expected for a (metal/degenerate semiconductor/metal) tunnel junction. Figure 2 contains a series of i–V curves taken directly over a GMM of MNOPE atop an n^{++}-Si(111) substrate. Note that the GMM had amine-topped molecules because they had not yet been converted to diazonium salts for reaction with C_{60} or SWCNTs. Unlike Fig. 1, several stepwise events, superimposed on a background current contributed from the direct electron tunneling between the tip and the n^{++}-Si substrate, are detected at both negative and positive tip bias. The stepwise currents in the positive tip bias region were observed in both forward and reverse scans. The behavior observed in each of the i–V curves was verified with multiple tips at different substrate locations, although the exact bias for stepwise events or current peaks varied from experiment to experiment with a standard deviation of $\sim \pm 0.2$ V. We have observed and reported[6] similar i–V behavior on self-assembled

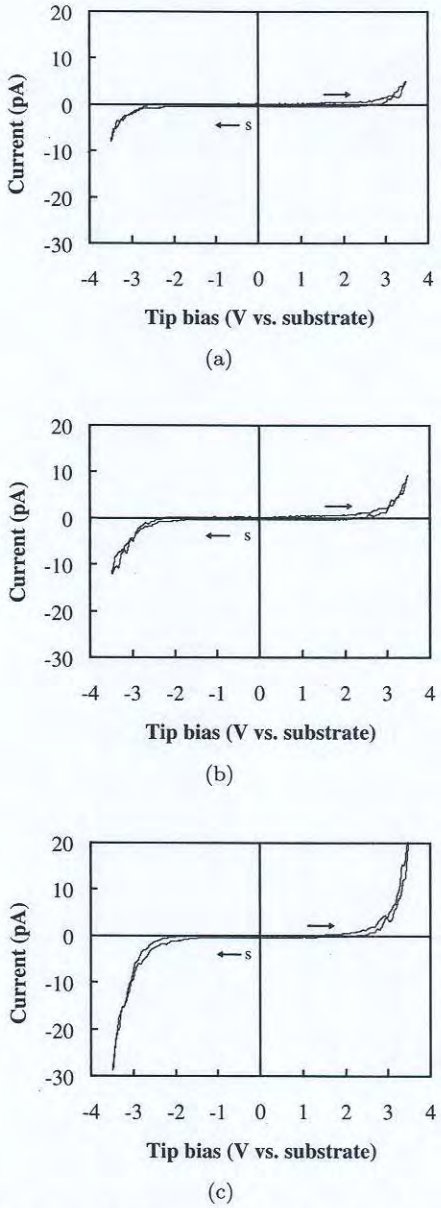

Fig. 1. A series of i–V curves taken at three different distances in 1.7 Å steps (from frame (a) to (b) and from frame (b) to (c)) as the tip approaches a hydrogen-terminated bare n^{++}-Si(111) surface. Potentials represent tip bias versus n^{++}-Si(111) substrate and all scans were taken from 0 V first towards negative bias, then to positive values and finally back to zero. $S \rightarrow$ stands for the starting point of the voltage scan and the initial scan direction.

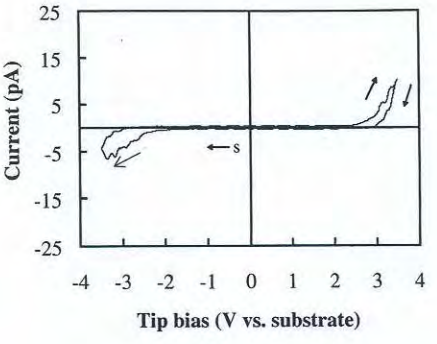

(a)

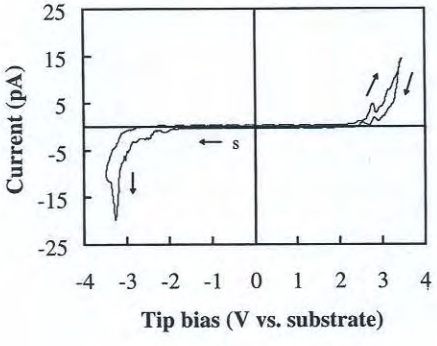

(b)

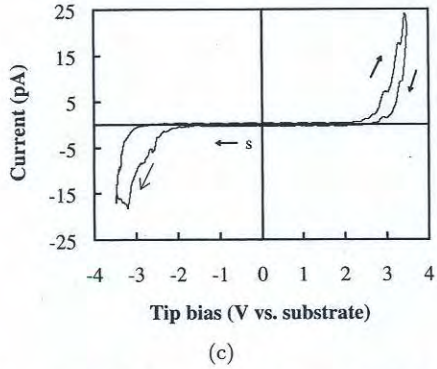

(c)

Fig. 2. A series of i–V curves taken at three different distances in 1.7 Å steps (from frame (a) to (b) and from frame (b) to (c)) as the tip approaches the surface of a GMM of MNOPE atop an n^{++}-Si(111) substrate. Potentials represent tip bias versus n^{++}-Si(111) substrate and all scans were taken from 0 V first towards negative bias, then to positive values and finally back to zero. $S \rightarrow$ stands for the starting point of the voltage scan and the initial scan direction.

monolayers (SAMs) of a similar thiolated nitro-compound on Au, although alkylthiol (RSH)/Au shows a relatively low background current from direct tunneling between tip and substrate and showed a lower threshold voltage (V_{TH}) for resonant tunneling (RT). A significant contribution of the potential drop across the space charge layer of a semiconductor as compared to a metal may contribute to the more negative V_{TH} with Si.

The observed i–V behavior is consistent with a RT mechanism recently proposed by Datta *et al.*[3] and by Hersam and coworkers.[3] Figure 3 schematically illustrates energy band diagrams that

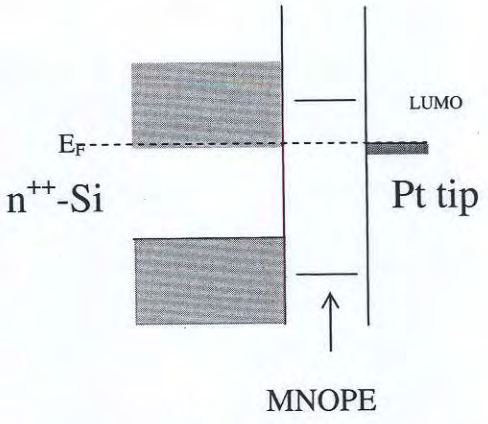

(a) At equilibrium

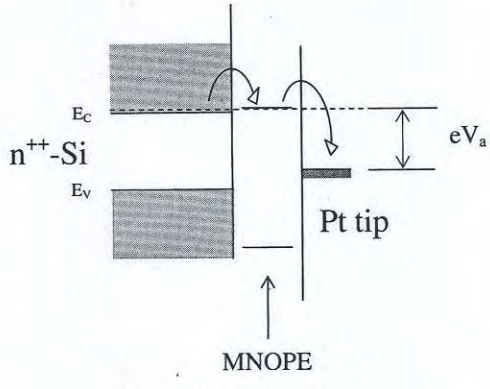

(b) High positive tip bias

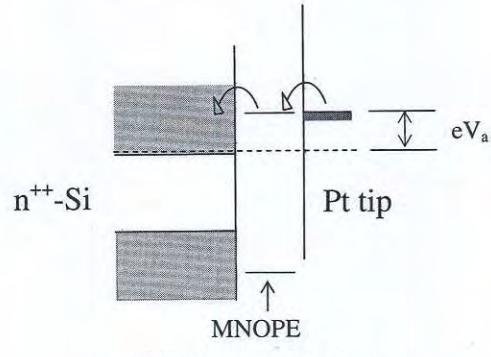

(c) High negative tip bias

Fig. 3. Energy band diagrams that summarize the charge transport mechanism of the (n^{++}-Si/MNOPE/Pt-tip) junction: (a) at equilibrium; (b) at high positive tip bias; and (c) at high negative tip bias. E_F: the Fermi level; E_C: the conduction band edge and E_V: the valence band edge of the n^{++}-Si(111) substrate. LUMO: the lowest unoccupied molecular orbital of MNOPE and V_a is the tip bias. The curved arrows represent electron hopping at the interfaces.

summarize the charge transport mechanism. Figure 3(a) shows equilibrium band diagrams for the (n^{++}-Si/MNOPE/Pt-tip) junctions. For simplicity, band bending at the silicon surface is not shown at the silicon surface, although the degree of band bending may play some role on the V_{TH} values observed, as mentioned above. The interfacial dipole and space charge layers at each interface which are important for the interfacial charge transfer processes, for simplicity, are also not shown in the figure.

The location of the Fermi level, E_F, with respect to the lowest unoccupied molecular orbital (LUMO) and the highest occupied molecular orbital (HOMO) of MNOPE is also not drawn to scale. Figure 3(b) considers the situation where a negative bias is applied to the n^{++}-Si substrate with respect to the grounded Pt-tip (or a positive bias of the tip with respect to the silicon substrate). At a critical applied bias, the electrochemical potential (μ_{Si}) of the Si substrate aligns with the LUMO of the MNOPE molecule, leading to RT and a peak in the conduction. At a bias slightly higher than this critical value, the narrow band of conduction electrons moves off resonance. Due to the presence of the conduction band edge, E_C, and the onset of the silicon band gap, the conduction at this bias level will decrease, leading to NDR. At even higher negative sample biases, μ_{Si} will move on and subsequently off resonance with higher unoccupied molecular orbitals. In agreement with the experimental data, this band diagram predicts multiple NDR events at negative sample bias. Figure 3(c) considers the situation where a negative bias is applied to the tip (versus the Si substrate). At a sufficiently high bias, the Fermi level of the Pt-tip aligns with the LUMO of the MNOPE molecule, leading to RT and a NDR peak could also be observed if one uses a very sharp Pt STM tip, which has narrow density of states around the Fermi edge as compared with a bulk electrode.[7] As shown in Fig. 2, significant hysteresis is also observed in the i–V curves: higher current flows through the junction in the forward scan as compared to the reverse scan, indicative of the presence of some charging (or electrochemical (EC)) processes.

Figure 4 shows a series of i–V curves for a (n^{++}-Si(111)/MNOPE/C_{60}/Pt-tip) junction. One striking difference between the i–V curves of this junction and those of the (n^{++}-Si(111)/Pt-tip) and (n^{++}-Si(111)/MNOPE/Pt-tip) junctions is the rectification: significant higher current was observed at negative tip bias as compared to the corresponding current at positive bias of the same magnitude at the same tip/substrate gap separation. For example, Fig. 4(b) shows a rectification ratio of ~ 10 at a bias of 3 V.

The observed i–V behavior was nearly independent of the initial voltage scan direction and the current showed no evident NDR peaks or shoulders but some hysteresis associated with the charging effect. Figure 5(I) schematically illustrates the energetics of the (n^{++}-Si/MNOPE/C_{60}/Pt-tip) interfaces that summarize the charge transport mechanism. Figure 5(I)(a) shows the equilibrium situation. The location of the Fermi level, E_F, with respect to the LUMO and the HOMO of MNOPE and C_{60} are not drawn in scale. However, we consider the relative positions of the LUMO of MNOPE with respect to the LUMO and LUMO + 1 of C_{60}, since they can affect the overall electron transport properties of the junction. We have previously shown that EC responses, e.g., half-wave reduction potential ($E_{1/2}$), correlated excellently with both theoretical LUMOs and experimental V_{TH}.[8] EC measurements of MNOPE in acetonitrile solution showed one reversible one-electron reduction wave at $E_{1/2} = -1.38$ V versus ferrocene/ferrocenium ($Fc/Fc+$)[8] and the $E_{1/2}$ measured for C_{60} in a mixed solvent of acetonitrile and toluene (1:5) was -0.98 V versus $Fc/Fc+$ for the first reversible one-electron reduction and -1.37 V for the second reversible one-electron reduction.[9] Thus, the LUMO level of MNOPE is well above LUMO of C_{60} but matches well with its LUMO+1 level, as shown in Fig. 5(I)(a). Figure 5(I)(b) considers the situation where a negative bias is applied to the n^{++}-Si substrate with respect to the grounded Pt-tip. At a critical applied bias, the electrochemical potential (μ_{Si}) of the Si substrate aligns well with the LUMO of the MNOPE molecule, leading to effective electron transfer (ET) from n^{++}-Si to MNOPE. Under these conditions, ET from n^{++}-Si to MNOPE and from the reduced MNOPE to C_{60} is quite feasible, although ET from n^{++}-Si to MNOPE does not occur easily at low negative bias. Figure 5(I)(c) considers the situation where a negative bias is applied to the tip (versus the Si substrate). At a sufficiently high bias, the Fermi level of the Pt-tip aligns well with the LUMO level of the C_{60} molecule, leading to C_{60} reduction; however, due to the mismatch of two LUMO levels, ET from reduced C_{60} to MNOPE

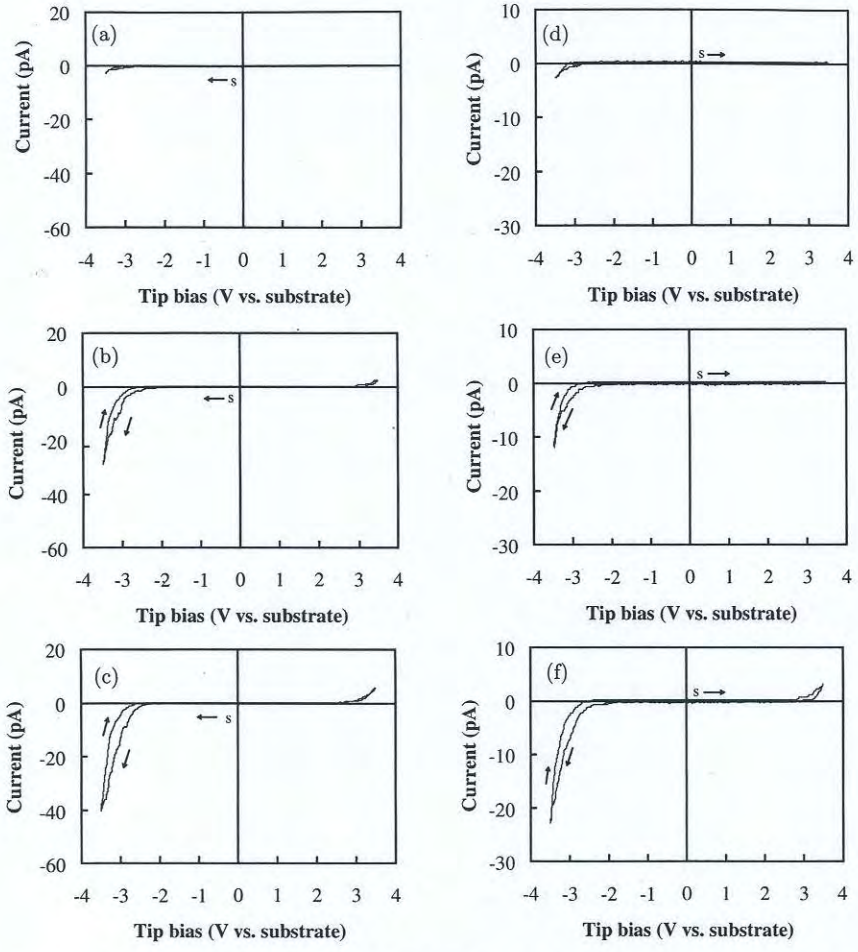

Fig. 4. A series of i–V curves for a (n^{++}-Si(111)/MNOPE/C_{60}/Pt-tip) junction taken at three different distances in 1.7 Å steps (from (a) to (b) and from (b) to (c) or from (d) to (e) and from (e) to (f)) as the tip approaches the surface of C_{60}. In frames (a), (b) and (c), the tip bias (versus n^{++}-Si(111) substrate) was scanned from 0 V towards negative bias, then to positive values and finally back to zero. In frames (d), (e) and (f), the tip bias was scanned from 0 V towards positive bias, then to negative values and finally back to zero.

is inhibited until the Fermi level of the Pt-tip aligns with the LUMO + 1 level of C_{60}. This leads to the formation of C_{60}^{2-} and thus feasible ET from C_{60}^{2-} to MNOPE and from the reduced MNOPE to n^{++}-Si substrate could take place.

Figure 6 shows a series of i–V curves for a (n^{++}-Si(111)/MNOPE/SWCNT/Pt-tip) junction. More than 30 junctions of this type were characterized and a majority ($\sim$60%) of the junctions examined show strong current rectification with much higher current observed at a positive tip bias as compared to the current flow at the negative bias of the same magnitude at the same tip/substrate gap separation. The rectification ratio, as shown, can reach high as 1000 at a bias of 3 V, as shown in Fig. 6(c). Notice that the polarity of the rectification of the SWCNT junctions is independent of the initial scan direction and is opposite to that observed for the fullerene junctions as discussed above. It is also interesting to point out that besides showing rectification, some of the junctions also show strong hysteresis in the i–V curves: higher current flows through the junction in the forward scan as compared to the reverse scan, indicative of the presence of some charging (or EC) processes. One might rationalize these rectifying i–V curves based on the interfacial energetics of the (n^{++}-Si/MNOPE/SWCNT/Pt-tip) junctions as shown in Fig. 5(II). Figure 5(II)(a) schematically illustrates the energetics of the (n^{++}-Si/MNOPE/SWCNT/Pt-tip) interfaces at thermodynamic equilibrium. SWCNTs are mixtures of metallic (0 eV band gap) narrow band gap semimetals (meV band gaps) or semiconductor with

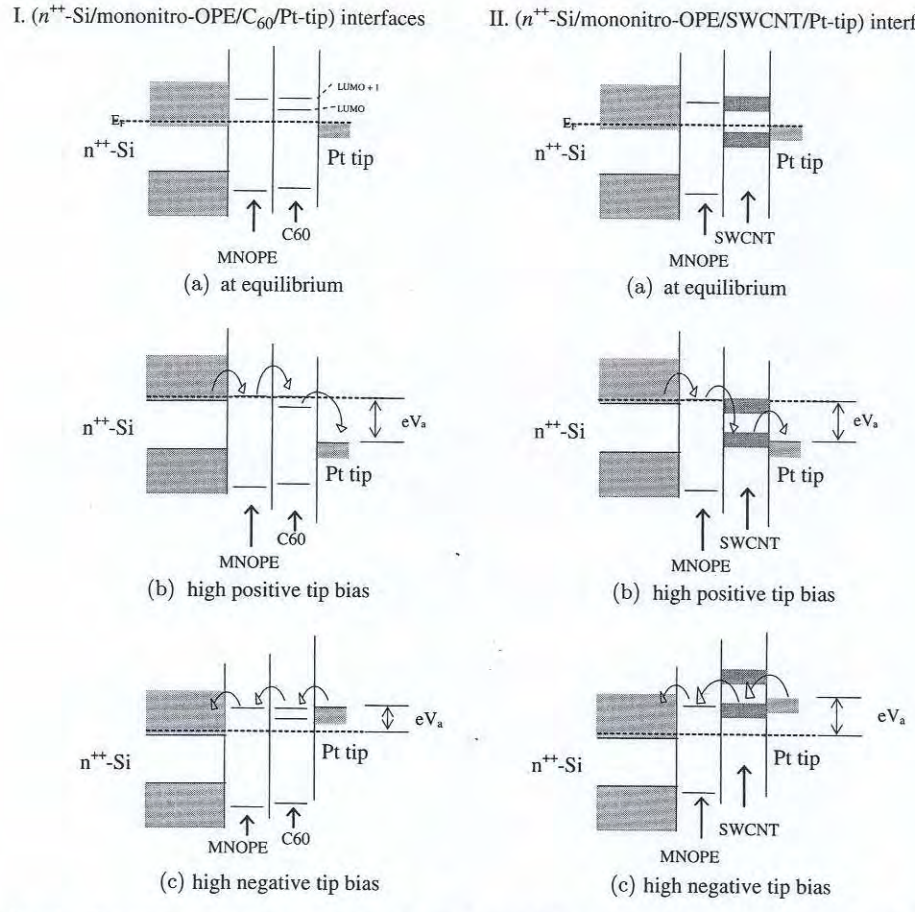

Fig. 5. Energy band diagrams that summarize the charge transport mechanisms of the (n^{++}-Si/MNOPE/C_{60}/Pt-tip): (I) and (n^{++}-Si/MNOPE/SWCNT/Pt-tip) (II) junctions: (a) at equilibrium; (b) at high positive tip bias; and (c) at high negative tip bias. E_F: the Fermi level; LUMO and LUMO + 1: the lowest and the next lowest unoccupied molecular orbitals of C_{60} and V_a is the tip bias. The curved arrows represent electron hopping at the interfaces.

a band gap, $E_g = 0.9\,\text{eV}/d[\text{nm}]$, where d is the diameter of the tube, and the HiPco derived tubes used here are approximately two thirds semiconducting and one third metallic/semimetallic.[10−12] Semiconducting SWCNTs are typically p-type because of the contacts and also because chemical species, particularly oxygen, adsorb on the tube and act as weak p-type dopants.[13] Thus, the (n^{++}-Si/MNOPE/SWCNT) structure can act as an n^{++}-i-p junction and the Pt-tip makes good contact to the SWCNT. At equilibrium, the Fermi level of Pt will align with the electrochemical potentials of n^{++}-Si and SWCNT. As a negative bias is applied to the n^{++}-Si substrate with respect to the grounded Pt-tip, at a critical applied bias as shown in Fig. 5(II)(b), the electrochemical potential (μ_{Si}) of the Si substrate aligns with the LUMO of the MNOPE molecule, leading to effective ET from n^{++}-Si to MNOPE and from the reduced MNOPE to SWCNT, where fast recombination of electrons and holes takes place. This is the forward-bias situation of a hetero n^{++}-i-p junction. As a low positive bias is applied to the n^{++}-Si substrate (versus the tip), both n^{++}-Si and SWCNTs (assuming it is a weak p-type semiconductor) are reverse-biased and thus negligibly small current will flow through the junction. However, at sufficiently high negative tip bias, as shown in Fig. 5(II)(c), the valence band edge of SWCNTs could match with the LUMO of MNOPE, leading to RT and the current flow will strongly depend on the doping level of the SWCNT. About 15% of the total junctions examined show i–V behaviors more or less similar to those of the (n^{++}-Si(111)/MNOPE/Pt-tip) junctions, suggesting the absence of SWCNTs at those locations.

Finally, a small, but significant, fraction ($\sim$20%) of the total junctions tested show switching behavior in the high current operating regime, whereas the (n^{++}-Si/MNOPE/Pt-tip) and (n^{++}-Si/MNOPE/C_{60}/Pt-tip) junctions did not

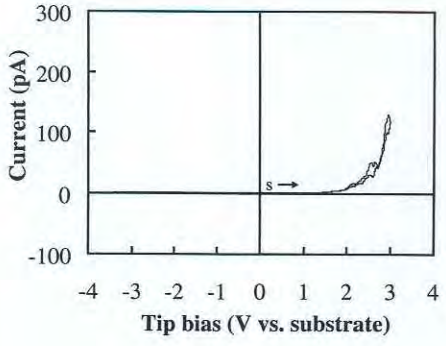

(a)

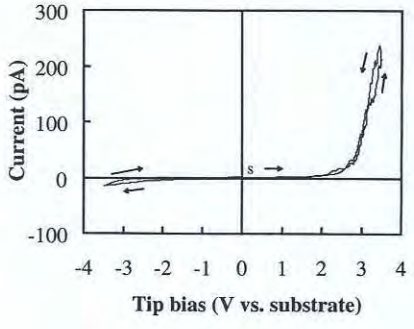

(b)

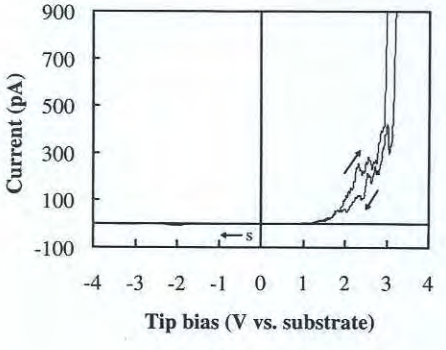

(c)

Fig. 6. (a) and (b): two consecutive i–V curves for a (n^{++}-Si(111)/MNOPE/SWCNT/Pt-tip) junction taken at two different tip distances at the same substrate location. Tip position in (b) is 1.7 Å closer to the substrate surface as compared to that in (a). In frames (a) and (b), the tip bias (versus n^{++}-Si(111) substrate) was scanned from 0 V towards positive bias, then to negative values and finally back to zero. (c): another i–V curve at different substrate location and the tip bias was scanned from 0 V towards negative bias, then to positive values and finally back to zero.

exhibit similar voltage-triggered switching. As shown in Fig. 7, as the tip bias is scanned from 0 to a low voltage ($V_a < 1.5$ V), negligibly small current flows through the (n^{++}-Si/MNOPE/SWCNT/Pt-tip) junction. The current then increases slowly

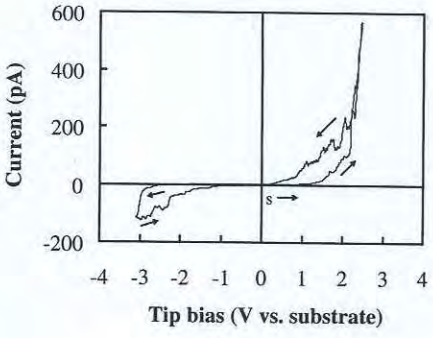

(a)

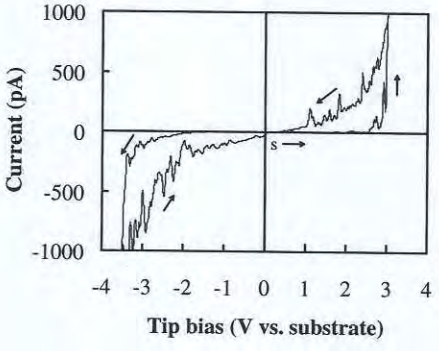

(b)

Fig. 7. Two i–V curves for a (n^{++}-Si(111)/MNOPE/SWCNT/Pt-tip) junction taken at two different substrate locations. The tip bias (versus n^{++}-Si(111) substrate) was scanned from 0 V towards positive bias, then to negative values and finally back to zero.

with increasing positive bias until a sharp increase in current at a threshold tip bias near $\sim 2.5 \pm 0.5$ V. The junction remains in the high current state as the tip bias keeps increasing to the upper boundary of the sweep voltage, where the current values sometime exceed 1 nA (the saturation current of the preamplifier), as shown in Fig. 7(b). In the reverse scan, the current stays substantially higher than the value observed in the forward scan but the magnitude decreases with more negative bias. The current returns to zero as the bias restores to its origin. As the tip bias is continuously scanned from 0 to a low negative voltage ($V_a > -2$ V), essentially no current flows through the junction. The current then increases monotonically until a sharp increase in current at a threshold tip bias near $\sim -3.3 \pm 0.3$ V. In the reverse scan, the junction remains in the high current state and the current decreases with decreasing negative bias. The current returns to zero as the bias returns to its origin. This type of switching behavior has most recently been observed for several

different molecules in a (metal/molecule/metal) junction. Several mechanisms have been proposed trying to interpret a molecular switching mechanism, including molecular conformational changes with charge redistribution,[14,15] formation of metal nanofilaments,[16] metal–molecule contact interruptions,[17,18] liquid crystal phase transition[19] and rotaxane-based switching.[20,21] The continuous change of current with respect to bias, except near the threshold turn-on voltage, as shown in our data, does not support metal–molecule contact breaking or metal nanofilment as the dominant mechanism responsible for the switching behavior observed here. Both mechanisms will predict a random and hysteretic on-off conduction, which seems to be independent of the applied voltage. Since both MNOPE and SWCNT are chemically stable and have robust structure, it is also not very likely those molecules will undergo substantial conformation change or phase transition to dramatically affect the conduction of the junction. However, charge injection and lateral transport via the SWCNTs are possible.

In summary, we report the observation of i–V characteristics for several (n^{++}-Si/MNOPE/C_{60}/Pt-tip) or (n^{++}-Si/MNOPE/SWCNT/Pt-tip) junctions. A layer of C_{60} or SWCNT-derivatized on MNOPE has strong effect on the i–V behavior of the junctions, including rectification, NDR and switching phenomena. Different i–V behavior was rationalized based on different interfacial energetics for electron transfer. Some of the (n^{++}-Si/MNOPE/SWCNT/Pt-tip) junctions also show monostable or reversible bistable switching behavior, whose mechanism is still unclear and yet to be resolved. The marriage of fullerene structures to silicon via an electroactive molecular system could provide an approach to the modification of silicon devices for modified switching and memory applications. The studies here underscore the new and robust electrical phenomena attainable from these novel interfacial hybrid Si/molecule/fullerene structures.

Acknowledgments

The support of this work by the National Science Foundation (CHE 0451494), the Defense Advanced Research Projects Agency, the Robert A. Welch Foundation and Molecular Electronics Corp. is gratefully acknowledged.

References

1. J. M. Tour, *Molecular Electronics: Commercial Insights, Chemistry, Devices, Architecture and Programming* (World Scientific, River Edge, NJ, 2003).
2. A. Nitzan and M. A. Ratner, *Science* **300**, 1384 (2003).
3. R. A. Wolkow, *Jpn. J. Appl. Phys.* **40**, 4378 (2001); M. C. Hersam, N. P. Guisinger and J. W. Lyding, *Nanotechnology* **11**, 70 (2000); N. P. Guisinger, R. Basu, M. E. Greene, A. S. Baluch and M. C. Hersam, *Nanotechnology* **15**, S452 (2004); T. Rakshit, G.-C. Liang, A. W. Ghosh and S. Datta, *Cond-Mat.* **1**, 0305695 (2003); S. Lenfant, C. Krzeminski, C. Delerue, G. Allan and D. Vuillaume, *Nano Lett.* **3**, 741 (2003); N. P. Guisinger, M. E. Greene, R. Basu, A. S. Baluch and M. C. Hersam, *Nano Lett.* **4**, 55 (2004).
4. M. P. Stewart, F. Maya, D. V. Kosynkin, S. M. Dirk, J. J. Stapleton, C. L. McGuiness, D. L. Allara and J. M. Tour, *J. Am. Chem. Soc.* **126**, 370 (2004); J. He, B. Chen, A. K. Flatt, J. J. Stephenson, C. D. Doyle and J. M Tour, *Nature Mater.* **5**, 63 (2006).
5. A. K. Flatt, B. Chen and J. M. Tour, *J. Am. Chem. Soc.* **127**, 8918 (2005); B. Chen, A. K. Flatt, H. Jian, J. L. Hudson and J. M. Tour, *Chem. Mater.* **17**, 4832 (2005).
6. F.-R. F. Fan, J. Yang, L. Cai, D. W. Price, Jr., S. M. Dirk, D. V. Kosynkin, Y. Yao, A. M. Rawlett, J. M. Tour and A. J. Bard, *J. Am. Chem. Soc.* **124**, 5550 (2002).
7. Y. Xue, S. Datta, S. Hong, R. Reifenger, J. I. Henderson and C. P. Kubiak, *Phys. Rev. B* **59**, R7852 (1999).
8. F.-R. F. Fan, R. Y. Lai, J. Cornil, Y. Karzazi, J.-L. Brédas, L. Cai, L. Cheng, Y. Yao, D. W. Price, Jr., S. M. Dirk, J. M. Tour and A. J. Bard, *J. Am. Chem. Soc.* **126**, 2568 (2004).
9. L. Echegoyen and L. E. Echegoyen, *Acc. Chem. Res.* **31**, 593 (1998).
10. P. L. McEuen, M. Fuhrer and H. Park, *IEEE Trans. Nanotechnolgy* **1**, 78 (2002).
11. T. W. Odom, J.-L. Huang, P. Kim and C. M. Lieber, *Nature* **391**, 62 (1998).
12. J. W. G. Wildoer, L. C. Venema, A. G. Rinzler, R. E. Smalley and C. Dekker, *Nature* **391**, 59 (1998).
13. J. Kong, N. R. Franklin, C. Zhou, M. G. Chapline, S. Peng, K. Cho and H. Dai, *Science* **287**, 622 (2000).
14. A. S. Blum, J. G. Kushmerick, D. P. Long, C. H. Patterson, J. C. Yang, J. C. Henderson, Y. Yao, J. M. Tour, R. Shashidhar and B. Ratna, *Nature Mater.* **4**, 167 (2005).
15. L. Cai, M. A. Cabassi, H. Yoon, O. M. Cabarcos, C. L. McGuiness, A. K. Flatt, D. L. Allara, J. M. Tour and T. S. Mayer, *Nano Lett.* **5**, 2356 (2005).

16. J. M. Tour, L. Cheng, D. P. Nackashi, Y. X. Yao, A. K. Flatt, S. K. St. Angelo, T. E. Mallouk and P. D. Franzon, *J. Am. Chem. Soc.* **125**, 13279 (2003).
17. G. K. Ramachandran, T. J. Hopson, A. M. Rawlett, L. A. Nagahara, A. Primak and S. M. Lindsay, *Science* **300**, 1413 (2003).
18. P. A. Lewis, C. E. Inman, Y. X. Yao, J. M. Tour, J. E. Hutchison and P. S. Weiss, *J. Am. Chem. Soc.* **126**, 12214 (2004).
19. S. Palto, L. Blinov, E. Dubovik, V. Fridkin, N. Petukhova, A. Sorokin, K. Verkhovskaya, S. Yudin and A. Zlatkin, *Europhys. Lett.* **34**, 465 (1996).
20. R. A. Bissell, E. Cordova, A. E. Kaifer and J. F. Stoddart, *Nature* **369**, 133 (1994); V. Balzani, A. Credi, S. J. Langford, F. M. Raymo, J. F. Stoddart and M. Venturi, *J. Am. Chem. Soc.* **122**, 3543 (2000); C. P. Collier, G. Mattersteig, E. W. Wong, Y. Luo, K. Beverly, J. Sampaio, F. M. Raymo, J. F. Stoddart and J. R. Heath, *Science* **289**, 1172 (2000).
21. M. Feng, X. Guo, X. Lin, X. He, W. Ji, S. Du, D. Zhang, D. Zhu and H. Gao, *J. Am. Chem. Soc.* **127**, 15338 (2005).